EMBRY-RIDDLE
Aeronautical University™
SCHOLARLY COMMONS

Dissertations and Theses

12-2012

Identification and Classification of Stratospheric Sudden Warming Events

Thomas S. Ehrmann
Embry-Riddle Aeronautical University - Daytona Beach

Follow this and additional works at: https://commons.erau.edu/edt

Part of the Atmospheric Sciences Commons, and the Climate Commons

Identification and Classification of Stratospheric Sudden Warming Events

by

Thomas S. Ehrmann

A thesis submitted to the

Physical Sciences Department

in partial fulfilment of the requirements for the degree of

Master of Science in Engineering Physics

Embry-Riddle Aeronautical University

Daytona Beach, Florida

December 2012

IDENTIFICATION AND CLASSIFICATION OF STRATOSPHERIC SUDDEN WARMING EVENTS

by

Thomas Ehrmann

This thesis was prepared under the direction of the candidate's thesis committee chair, Dr. John M. Hughes, Department of Physical Sciences, and has been approved by the members of the thesis committee. It was submitted to the Department of Physical Sciences and was accepted in partial fulfillment of the requirement of the Degree of

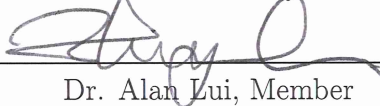Masters of Science in Engineering Physics

THESIS COMMITTEE

_____
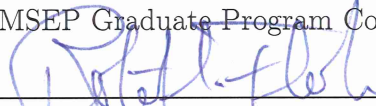Dr. John M. Hughes, Chair

_____
Dr. Jonathan B. Snively, Member
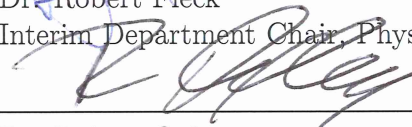
_____
Dr. Alan Lui, Member

_____
Dr. Peter Erdman
MSEP Graduate Program Coordinator

_____
Dr. Robert Fleck
Interim Department Chair, Physical Sciences

_____
Dr. Robert Oxley
Associate Vice President for Academics

_____
3/5/2013
Date

iii

Abstract

Analysis of northern hemisphere stratospheric data from 1978-2011 is used to identify and classify Stratospheric Sudden Warming events. A total of 41 events are identified during this 33 year period, resulting in an average occurrence rate of 1.24 events/year. No significant variation in the rate is observed during the period analyzed. The average temperature increase during an SSW event is 12 K and the average duration is 32 days. Each identified event is classified as either a vortex displacement or split event and the ratio of displacement to split events is found to be 0.86.

Acknowledgements

Most importantly, I would like to thank my family for all the support they have given me over the years, especially my parents for always encouraging me to pursue my passions. I also want to thank my advisor, Dr. Hughes, for helping guide me through my time at Embry-Riddle, and for allowing me the freedom to change the direction of this thesis as my interests evolved. I want to thank the committee members for their advice and their patience and, I would like to thank the Engineering Physics program at Embry-Riddle for providing me with an interesting and nuturing environment to learn in during my time here. Additionally, I want to thank my peers working in the Space Physics Research Lab for keeping me entertained and providing good company while I completed this thesis. And lastly, I would like to thank myself because through me all things are possible.

Contents

List of Tables

List of Figures

Chapter 1

Introduction

1.1 Neutral Atmosphere

The neutral atmosphere is the layer of non-ionized atoms and molecules that surround the Earth. This layer extends up well past 1000 km; however, the vast majority of it exists below one hundred kilometers, as pressure and density decreases exponentially with altitude. The neutral atmosphere is divided up into several layers, based on the way temperature changes with altitude in those regions. The bottom layer is the troposphere; it starts at sea-level and extends up to the tropopause at approximately 10 km. This layer cools from about 300 K ($\sim 25\,°\text{C}$) down to as low as 200 K (Hughes, 2008). After the tropopause the atmosphere begins to warm again with altitude due to the presence of ozone absorbing radiation from the sun. This layer, known as the stratosphere, extends up to approximately 45 km, and reaches temperatures around 270 K at the stratopause (Hughes, 2008). The next layer of the atmosphere is known as the mesosphere, once again undergoing cooling with an increase in altitude.

The mesosphere reaches the coldest temperatures achieved in our atmosphere at the mesopause, which is around 180 K at approximately 80 km (Hughes, 2008). The final layer of the neutral atmosphere is known as the thermosphere; this layer extends up into space, with temperature increasing exponentially. The highest temperatures in the neutral atmosphere occur in the thermosphere because it receives the majority of the sun's radiation, and density is very low so that less energy is needed to affect the temperature (Hughes, 2008).
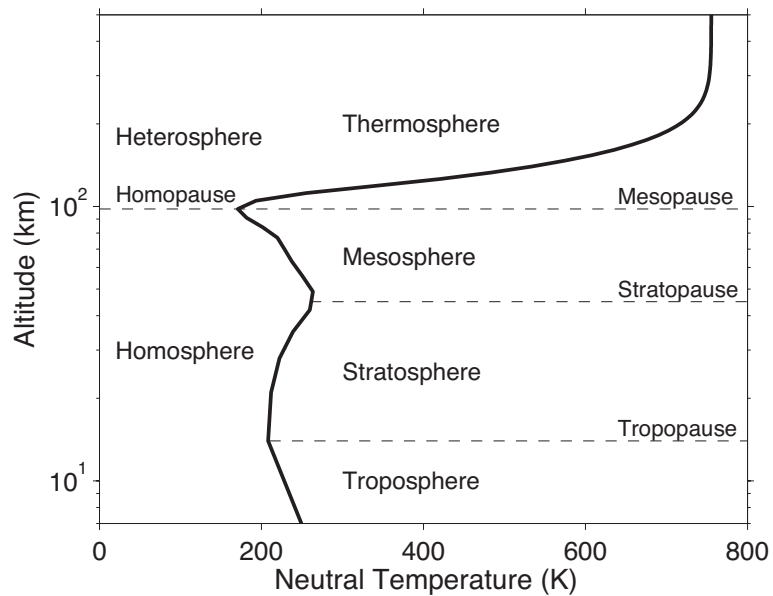
Figure 1.1: A typical graph of temperature versus altitude along with labeling of separate regions in neutral atmosphere (Hughes, 2008)

1.2   Atmospheric Dynamics

This report is based on complex weather events over the north pole, during which large vortices in the upper atmosphere experience very sudden and dramatic dynamic changes. These dynamic phenomena involve important changes to both the temperature and wind fields over the pole, and are known as stratospheric sudden warming events. Throughout the next several sections, basic concepts and parameters will be described to help understand the dynamics of the neutral atmosphere. These concepts will then be combined to help explain the physical causes and effects of the stratospheric sudden warming events.

1.2.1   Geostrophic Balance

Geostrophic balance is the assumption that the wind vectors in a certain region are parallel to the contour surface of constant pressure at that level. This assumption is a result of horizontal forces coming into balance. Specifically, when the pressure gradient force acting on a particular air parcel is balanced by the Coriolis force that parcel is considered to be in geostrophic balance (Mak, 2011). This assumption becomes more valid at higher latitudes, where the influence of the Coriolis force is greater, and is most appropriate when there is little variation in the direction of the wind. Almost all atmospheric wind data is given based on pressure levels instead of altitudes, making the geostrophic balance assumption very useful in practice.

1.2.2 Vorticity and Circulation

It is very common for wind flowing through the atmosphere to form both large and small cyclone-like patterns. This cyclonic wind pattern is known as an eddy. In order to understand the motion and evolution of these eddies, along with all circular flow throw the atmosphere, two different rotational properties are used. The first is vorticity, which is defined as the curl of the wind velocity vector.

$$\vec{\zeta} = \nabla \times \vec{V} \tag{1.1}$$

Vorticity is a vector that points perpendicular to the rotation of the fluid based on the so-called "right-hand rule." A useful variation on vorticity is known as absolute vorticity, this is also the curl of the velocity but it takes into account the influence of the Earth's rotation $\vec{\zeta}_{absolute} = 2\vec{\Omega}\sin\varphi + \vec{\zeta}$, where $\vec{\Omega}$ is the angular velocity of the Earth aligned with the rotational axis and φ is the latitude (Mak, 2011).

The second useful rotational property is circulation. Circulation, C, is a scalar quantity that represents the strength of the wind along a certain path, Γ. It is defined as the line integral of the tangential component of the velocity along a closed loop.

$$C = \oint_{\Gamma} \vec{V} \cdot d\vec{\ell} \tag{1.2}$$

The circulation along a path that lies on the surface of a vortex and encloses the entire vortex can be thought of as a measurement of the strength of that vortex. It is important to point out the relationship between circulation and vorticity. The

definition of Stokes' theorem is:

$$\oint_{\Gamma} \vec{V} \cdot d\vec{\ell} = \int\int_A (\nabla \times \vec{V}) \cdot \vec{n}\, da \tag{1.3}$$

where A is the area enclosed by path Γ, and $\vec{n}$ is a vector normal to the discrete area da. Using this the following relationship can be derived:

$$C = \int\int_A \vec{\zeta} \cdot \vec{n}\, da \tag{1.4}$$

1.2.2.1 Vorticity Equation

It is useful to understand the way vorticity evolves in the atmosphere over time. To do this the equation for rate of change for vorticity at any point will be found. Start with the momentum equation for neutral atmosphere, as shown below (Mak, 2011).

$$\frac{\partial \vec{v}}{\partial t} = -\vec{v} \cdot \nabla \vec{v} - 2\vec{\Omega} \times \vec{v} - \frac{\nabla p}{\rho} + \vec{g} + \vec{F} \tag{1.5}$$

Here $\vec{g}$ is the acceleration due to gravity and $\vec{F}$ is the frictional force per unit mass. By using several vector identities and taking the curl of both sides a general form for the vorticity equation is obtained (Mak, 2011).

$$\frac{\partial \vec{\zeta}}{\partial t} = -(\vec{v} \cdot \nabla)\vec{\zeta_a} + (\vec{\zeta_a} \cdot \nabla)\vec{v} - \vec{\zeta_a}\nabla \cdot \vec{v} + \frac{\nabla \rho \times \nabla p}{\rho^2} + \nabla \times \vec{F} \tag{1.6}$$

5

In this equation $\vec{\zeta}_a$ is the absolute vorticity, as it is defined above. The most important term in this equation for this research is the baroclinic effect, $\frac{\nabla\rho\times\nabla p}{\rho^2}$. When the pressure gradient and temperature gradient are parallel this term goes to zero and the fluid is barotropic. However, for reasons that will be explained later, this term is very important in describing the vorticity at higher latitudes.

1.2.2.2 Potential Vorticity

Another interesting variation on vorticity in called Ertel's potential vorticity, which is defined as:

$$ q \equiv \frac{\vec{\zeta}_a \cdot \nabla\theta}{\rho} \,. \tag{1.7} $$

The θ in this equation is for potential temperature, which is the temperature an air parcel would have if it were adiabatically brought to a reference pressure P_0 (usually 1000 mb).

$$ \theta = T\left(\frac{P_0}{P}\right)^{\frac{R}{c_p}} \tag{1.8} $$

Here R is the gas constant, and c_p is the specific heat capacity at a constant pressure. For a rotating flow in a compressible fluid the potential vorticity at any point is conserved over time (Mak, 2011). This principle will be important later in understanding the mechanisms for Rossby waves.

1.2.3   Wintertime Polar Vortex

During the months of November to March, known as the extended wintertime season in the northern hemisphere, solar heating over the polar region is significantly diminished and causes a poleward decrease in temperature. Since temperature in a fluid in directly related to pressure this creates a pressure gradient in the meridional direction. This pressure gradient is perpendicular to density gradient, which is always vertictal, and a baroclinic effect is created as described above. This baroclinic shearing creates a strong westerly, or eastward, rotation (Mak, 2011). This can also be thought of in terms of the geostrophic assumption; the pressure gradient force pushing winds toward higher latitudes is balanced by the Coriolis force pushing wind toward lower latitudes and the wind is forced to move zonally, in this case westerly. The vortex created by this effect pushes warm air out to the edge causing the air above the pole to become increasingly colder, and making the flow more stable. This wind pattern is sometimes referred to as the polar night jet, but it will be referred to here as the polar vortex. The vortex starts at about $60\,^{\circ}$N and reaches a maximum zonal wind speed at an elevation of around 65 km (Mak, 2011).

1.2.4   Rossby Waves

A Rossby wave is a large scale atmospheric wave that is driven by the rotation of a body through a non-uniform potential vorticity. The potential vorticity in a general 2-D fluid model is the same as the absolute vorticity so for simplicity that will be the parameter used to explain the mechanism behind this wave (Mak, 2011). The absolute vorticity on the surface is a combination of the relative vorticity plus the

planetary vorticity, also known as the Coriolis parameter. The planetary vorticity, f, at some latitude φ is defined as:

$$f = 2\Omega \sin \varphi. \tag{1.9}$$

Now keeping in mind the notion that potential vorticity must be conserved, assume that some air parcel (A) in the northern hemisphere is displaced south, as demonstrated in Figure 1.2. This would decrease its planetary vorticity and cause an increase in the relative vorticity associated with that parcel, directly to the east. This would then cause the air parcel to the east of this increase in relative vorticity to be displaced north (B) where planetary vorticity is lower, again to conserve absolute vorticity. This process can also be thought of as a westward displacement of the vorticity. Because of the relationship between vorticity and velocity there is a westward movement of the sinusoidal pattern formed in the flow field. Therefore, all Rossby waves are associated with a westward, or easterly, phase velocity regardless of hemisphere. Rossby waves are formed on the scale of the Earth's circumference with the most critical waves having a zonal wave number of 1 or 2.

The largest flux of Rossby waves is found at mid-latitudes in the upper troposphere, particularly around 30° at the 200 mb level (10 km) (Mak, 2011). These waves are generated through topographical disturbances and complex eddy interactions, and are more prevalent in the northern hemisphere where the topography is more variant. There are two types of Rossby waves generated at these mid-latitudes, stationary waves and transient waves (Mak, 2011). The waves relevant to this research are the
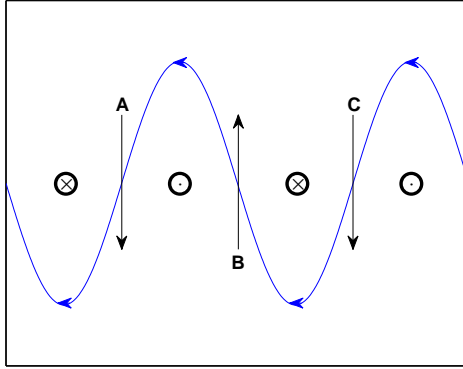
Figure 1.2: Shows the mechanisms of a Rossby wave. The black arrows show the displacement of air parcels, bold black circles mark the minimums and maximums in relative vorticity, and the blue line the resulting overall wind pattern

transient waves, particularly waves that travel north from these mid-latitudes.

1.2.5   Critical Level

When an atmospheric wave propagates into a region with a background mean flow $(\overline{U})$ it experiences a Doppler shift in frequency. If the propogation of the wave is aligned with the mean flow the equation for the Doppler shift is

$$\omega_o = \omega - k\overline{U} \tag{1.10}$$

where ω_o is the intrinsic frequency and k is the wave number (Hickey, 2011). It is possible for ω_o to be zero if the wave is propagating in the same direction as the mean flow. This is particularly relevant for waves where the frequency is very low, such as

9

Rossby waves. The layer in the atmosphere where $\omega_o = 0$ is known as the critical level because the wave is blocked from propagating further, and is absorbed by the background flow (Hickey, 2011). When a wave is absorbed at the critical level the energy and momentum associated with that wave also is absorbed. This can cause significant dynamic occurrences such as stratospheric sudden warming, which will be explained in the next section.

1.3 Stratospheric Sudden Warming

Since upward propagating Rossby waves also propagate poleward, these waves often encounter the wintertime polar vortex. The strength of the westerly vortex usually acts as a barrier to these easterly waves, refracting them toward the lower latitudes stratosphere where there effects are minimal (Mak, 2011). However, when there is an unusually high number of Rossby waves the flux of zonal momentum can weaken the westerly flow enough to allow waves to penetrate into the vortex. This penetration can only be achieved by Rossby waves of zonal number 1 or 2 because larger wave numbers do not possess the energy necessary (Matsuno, 1971).

This process was originally explained and modeled by Matsuno (1971). The waves initially propagate vertically into the high latitudes of the pole, while waves at lower altitudes increase in amplitude (Figure 1.3). All of this causes an easterly acceleration of the zonal flow throughout the vortex until eventually the mean zonal wind begin to reverse from westerly to easterly (Figure 1.4). This easterly flow begins first at high altitude where the acceleration is more efficient due to lower density, and creates a critical level for the Rossby waves. As the waves continue to propagate upward
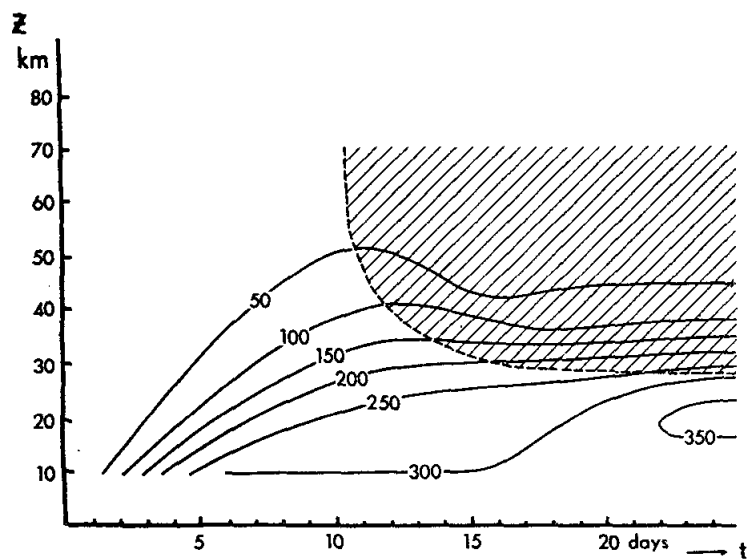
Fɪɢ. 4. The amplitude of disturbance at 60N as a function of time and height, case A. Hatched area indicates easterly mean flow.

Figure 1.3: Wave amplitude in millibars in a model SSW event. Model is driven by constant forcing function of number 2 waves with 300 mb amplitude. Critical layer marked by edge of hatched area (Matsuno, 1971).

they encounter the critical level, and deposit their energy and momentum into it as they are absorbed. This initially causes the critical level to grow downward in altitude very rapidly until it begins to stabilize due to the increasing pressure of the atmosphere. This formation of the critical layer and reversal of the zonal wind from westerly to easterly is associated with the deformation and eventual destruction of the polar vortex structure which will be discussed in the next section.
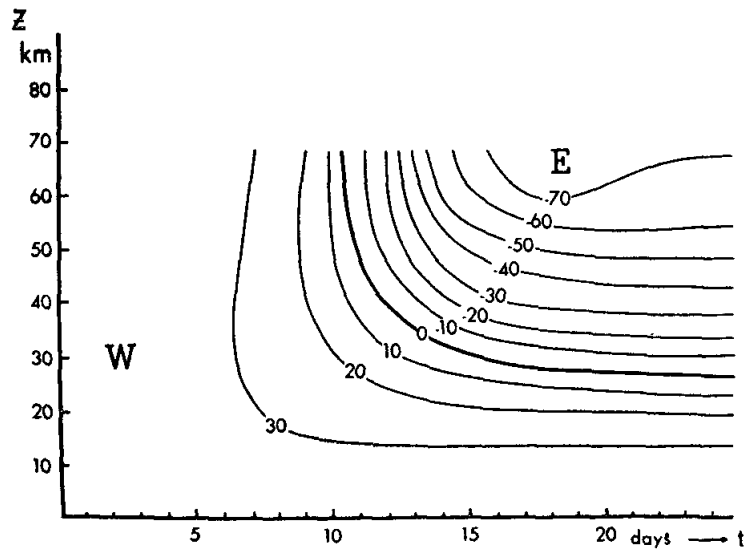
FIG. 5. Velocity of the mean zonal wind (m sec^{-1}) at 60N as a function of time and height, case A.

Figure 1.4: Zonal mean zonal wind in a model SSW event (Matsuno, 1971).

After the critical level has formed and become temporarily stable the actual "sudden warming" phenomenon begins. As the waves from lower altitudes with greater amplitudes interact with the critical level an incredible amount of energy in the form of heat is transferred into this high latitude region. This causes a dramatic temperature increase in and directly above the region occupied by the critical level (Figure 1.5),

12

and a complete reversal of the meridional temperature gradient since temperature increase is more dramatic closer to the pole. This phenomenon associated with increase in temperature over the pole, reversal of the meridional temperature gradient, the reversal of the zonal wind from westerly to easterly, and the breakdown of the polar vortex is known as a stratospheric sudden warming event (SSW). These SSWs are much more common in the northern hemisphere where topographical disturbances cause an increased presence of Rossby waves (Mak, 2011).
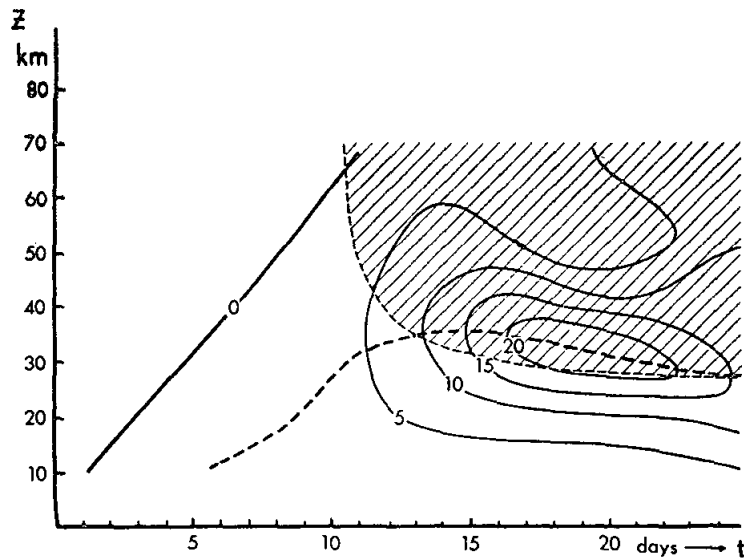
FIG. 6. Temperature (°C) at the pole as a function of time and height, case A. The thick dashed line shows the level of the maximum temperature rise. The easterly layer is hatched.

Figure 1.5: Temperature in a model SSW event. Critical layer marked by edge of hatched area (Matsuno, 1971).

SSWs have been shown to have dramatic effects on the troposphere and ground weather in the northern hemisphere. Warming begins in the upper stratosphere caus-

ing temperature and wind anomalies which propagate downward and exert a significant impact on storm tracks and the formation of troposheric jets, as well as creating an equatorward flux of heat and momentum in the weeks succeeding the event (Baldwin and Dunkerton, 1999; Limpasuvan et al., 2004). SSWs are also associated with signatures in the upper atmosphere. Warming in the stratosphere is often preceded by cooling in the mesosphere (Azeem et al., 2005). Studies have also indicated a correlation between SSWs and warming in the upper mesosphere and lower thermosphere as well as cooling in the thermosphere at altitudes as high as 300 km (Goncharenko and Zhang, 2008).

1.3.1 Displacement vs. Split

During a SSW the wintertime polar vortex temporarily disappears around the same time the mean zonal wind reverses from westerly to easterly. Before the vortex completely disappears it is deformed into some irregular shape as it begins to dissipate. During this deformation the vortex is generally considered to deform into one of two distinctly different ways. The first is when the vortex drifts away from the pole toward lower latitudes. This is known as a "displacement" type event, and it is characterized by the fact that the vortex deforms into a "comma" shape as it is weakening. The other type of event is when the vortex is split into two smaller vortexes and each of these drifts separately away from the pole before dissipating, such events are known as "split" type events. Each of these developments have distinctly different effects on lower atmospheric dynamics. Specifically, during a split event deformation of the vortex is distinctly barotropic, while during displacement events the vortex tilts west-

ward with altitude (Waugh and Polvani, 2010). It is not entirely clear what causes these two different scenarios. Often a correlation is made between the type of Rossby waves that caused the SSW and the type of event: if the waves which cause the event are mostly of wavenumber 1 it is a displacements, and if they are wavenumber 2 it is a split. However, there also seems to be some relationship to the preconditioning of the vortex before the event based on atmospheric blocking in lower layer of the atmosphere (Martius et al., 2009; Taguchi, 2008).

1.4   Motivation

The primary goal of this thesis will be to create a comprehensive list of all SSWs that occurred in the recent past (1978-2011) and then to classify each event as either a displacement or split. Several other studies have presented comprehensive catalogs of SSW events with the most recent being those of Charlton and Polvani (2007) and Tomikawa (2010). These catalogs focused on so-called major SSWs using the World Meteorological Organization (WMO) definition which requires reversal of the zonal mean zonal wind (ZMZW) at the 60 °N latitude, 10 hPa pressure level (McInturff, 1978). These catalogs include very few events from the 1990s and yield an average occurrence rate which is significantly different for that decade than for the surrounding ones.

An effort was also made to devise a more accurate and physically significant technique for identifying events. The main motivation behind this project will be to verify the results of previous efforts and create a more complete list of SSWs. The rate of events as well as the rate of displacements/splits where also checked. In addition to

this, there was some analysis of the temperature changes associated with each event as well as the duration of the events.

A more accurate and complete list of events is a useful tool for future research. The list of events also allows us to go back and look at data available from around the world coinciding with events. This allows us to gain a better understanding of the impact of an SSW, particularly in the mesophere and lower thermosphere where study of SSW impact is relatively new.

Chapter 2

Characterization of Stratospheric Sudden Warming Events

2.1 Event Identification

In order to identify SSW events, as well as classify each event, data from the National Centers for Environmental Prediction (NCEP)/National Center for Atmospheric Research (NCAR) Reanalysis Project will be used. These include, among other things, temperature, zonal wind and meridional wind at the 10 hPa level at resolutions of 4-times per day and 2.5 degrees in latitude and longitude. Here we restrict identifications to those events occurring in the years spanning 1978-2011 in order to avoid known inaccuracies, especially over the pole, due to the absence of satellite data in earlier years (Sturaro, 2003). Data from the extended winter season are analyzed, which is here defined as from November 1, 1978 to March 15, 2011.

Traditionally the World Meteorological Organization (WMO) definition for an

SSW is used to identify events. This definition makes a distinction between so-called "major warming" and "minor warming." Minor warming is defined as when the meridional temperature gradient reverses for five consecutive days, and major warming is when the zonal mean zonal wind (ZMZW) at the 60 °N latitude, 10 hPa pressure level reverses from westerly to easterly (McInturff, 1978). Because this is the standard definition, we originally only regard these identifications.
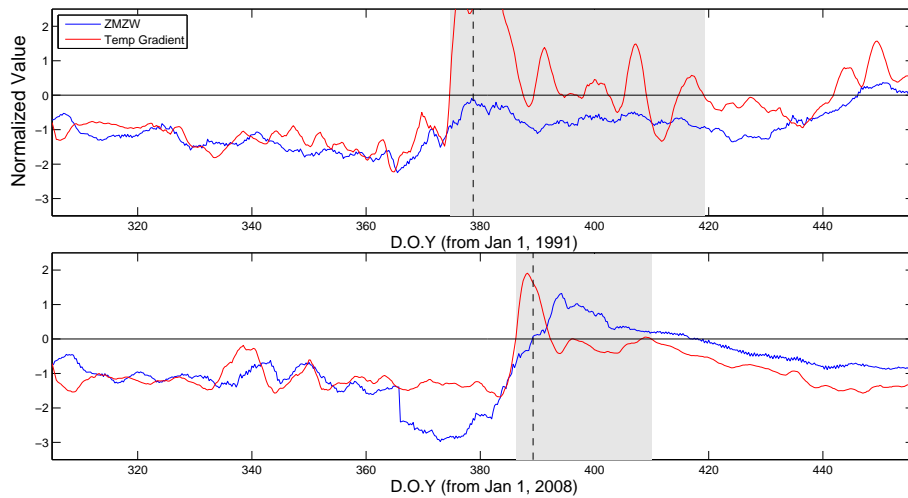
Figure 2.1: NCEP/NCAR stratospheric data from 10 hPa for the winters of 1991-1992 and 2008-2009 are displayed. The 1991-1992 event (on top) is a more traditional minor warming event, and the 2008-2009 event is a typical major warming event. ZMZW is taken from $70 - 80$ °N and is indicated by the blue line, and meridional temperature gradient in calculated from $60 - 90$ °N and is indicated by the red line. The central date for each event is marked by the vertical dashed line.

The meridional temperature gradient is obtained by computing the zonal mean temperature for all latitudes from $60 - 90$ °N, numerically evaluating the meridional

derivatives at each latitude, and then averaging them all together. As explained previously, temperature normally decreases in the meridional direction toward the pole so that these derivatives are normally negative, and a positive temperature gradient indicates the pole has warmed relative to the lower latitudes and is a strong indicator of an SSW event. This value is smoothed using a sliding average to eliminate variability. After some trial and error it is determined that an 8-point (2-day) sliding window is most effective. The ZMZW is originally obtained by numerically averaging the zonal wind component for all longitudes at $60\,°$N latitude. The winter seasons of 1991-1992 and 2008-2009 are each shown to demonstrate a typical minor and major warming event, respectively. Atmospheric parameters are displayed in Figure 2.1 with the ZMZW indicated by the blue line and the merdional temperature gradient by the red line; both values are oriented to become positive signalling an event. The temperature gradient reverses for both events, but the ZMZW does not pass the zero line during the 1992 event. It is important to note, however, that there is a disturbance in the ZMZW correlated with this minor warming event despite the fact that it never fully reverses. As it turns out, almost all minor warming events have some coorelated ZMZW disturbance assiciated with them which implies a more general identification process may be in order.

This observation of problems with the definition of major warmings and minor warmings seems to be in agreement with the conclusions of Coughlin and Gray (2009). Coughlin and Gray (2009) preformed a statistical analysis on stratospheric wind and temperature data around the wintertime North Pole to determine the number of distinct states that exist. They determined that the stratosphere either exist in a warmed and dynamically disturbed state, or a cooler undisturbed state. Because

19

of this no distinction will be made between major and minor warming in my final analysis. The ZMZW valued used in this identification process will be the average of the ZMZW from $70-80\,°$N because this is the value shown to be most associated with stratospheric disturbance by Coughlin and Gray (2009). This new ZMZW value is shown in Figure 2.1 where it is clearly correlated with disturbance in the temperature gradient. Unfortuantely, identifying events by when this new ZMZW value reverse still misses some clear disturbances, but if the ZMZW threshold for identifying an event is moved to a low westerly value nearly all minor warmings are identified. The specific criteria used here for identifying an SSW event are then as follows:

1. The meridional temperature gradient must reverse for a duration of at least 4 days.

2. The ZMZW must drop below 6 m/s westerly during the period starting 5 days before and ending 10 days after the duration of the temperture gradient reversal.

3. The first day that the ZMZW is easterly during the event, or the day of the lowest westerly ZMZW, is denoted the "central date" for the event.

4. No identifications subsequent to the central date are made for days prior to when the meridional temperature gradient has maintained undisturbed (negative) values for at least 15 consecutive days.

Each identified event is verified by observation of the time series. This verification is used to eliminate faulty identifications due, for example, to the annual presence of final warmings as the stratosphere returns to normal summertime conditions. Originally the extended winter season was taken to go from November 1 to March 31;

however, every warming that began after March 15 was dismissed as a final warming after observation. Therefore, the period used in this analysis will span from November 1 to March 15.

2.2   Additional Analysis

After the event is identified, additional analysis is performed using the temperature data to quantify the duration of the warming along with the intensity of the change in temperature and zonal wind. The duration of each event is defined using the same meridional temperature variable from the previous section. Given an identified SSW event, its duration is the time period between what will heretofore be referred to as the "initial reversal" and the "final return". The initial reversal is the date at which the meridional temperature gradient first reverses direction, and the final return is the last time the gradient returns to undisturbed (negative). To ensure consistency with criterion 4 from the previous section, the final return cannot occur until either at least 15 days of continuously undisturbed meridional temperature gradient values or the season's final warming. The final warming is when the northern stratosphere returns back to its summertime condition, and it is associated with a final reversal of the meridional temperature gradient at the end of the season.

After the duration is established for each SSW event the temperatures associated with the event are determined. An area-weighted average of all temperatures from $60 - 90\,^{\circ}$N latitude at the 10 hPa pressure level will be used as a measure of temperature for the stratosphere at any given moment. The average of all of these temperatures over the event's duration is computed and labeled as T_{ave}. The average

temperature is also computed for the two weeks prior to the event's initial reversal, and the difference between this and T_{ave} is defined as ΔT where a positive value indicates a warming during the event. This is a useful variable as it helps quantify the strength of the warming associated with each event. Next, the maximum area-weighted temperature is determined for each event's duration and labeled T_{max}. Finally, the maximum ZMZW value starting five days before the initial reversal and ending ten days after the final return is found, and recorded as $ZMZW_{max}$.

Chapter 3

Classification of SSW events

Each identified SSW event may be classified based on the evolution of the polar vortex, as described in Section 1.3.1, into a displacement event or a split event. The technique used here to do this classification closely follows that of Charlton and Polvani (2007) with minor modifications. In particular, the method used here to identify the vortex edge requires that it enclose the center of the main vortex and has a absolute vorticity value above the noise floor ($7 \times 10^{-5}\,s^{-1}$), instead of considering the distance from the vortex center to its edge. The geographical center of the main vortex is taken to be the location where the vorticity reaches its maximum value. Following Charlton and Polvani (2007), the period analyzed for each event spans from 5 days before through 10 days after the central date and analysis begins with identification of the vortex using absolute vorticity on a pressure surface, ζ_p. The specific classification scheme used here is as follows:

1. Compute ζ_p and identify Z_{max} as the location of max(ζ_p).

2. Compute $\nabla^2 \zeta_p$ and its mean absolute value along contours evenly spaced be-

tween $\max(\zeta_p)$ and the noise floor of ζ_p.

3. Identify the main vortex edge as the contour with the lowest mean absolute value of $\nabla^2\zeta_p$ that encloses Z_{max}. This and other contours at the same value are denoted vortex edges, Z_e.

4. Compute the circulation within each contour at the value of ζ_p on Z_e using Stokes' Theorem.

5. If the ratio of the second to the first highest circulation is ≥ 0.5 on more than one vorticity field during the period analyzed, the event is classified as a split and otherwise as a displacement.

6. All event classifications are confirmed by manual inspection of the ζ_p contours. The date for which ζ_p determines the classification is here denoted the event epoch.

A vortex is traditionally identified using the potential vorticity, however, absolute vorticity is approximately the same in describing the general form of the vortex and far simpler to calculate. Using the geostrophic approximation it is assumed that wind vectors are parallel to the pressure surfaces. This means that the vertical component of the curl of the wind on a pressure surface, known as ζ_p, is a reasonable substitute for describing the vortex's general morphology. This assumption is confirmed by the results of Baldwin and Holton (1988), where they showed contours of potential vorticity, and absolute vorticity (ζ_p) to confirm that the latter was sufficient for analyzing vortex form. As a test to confirm the accurracy of ζ_p, the contours of vorticity are plotted over velocity vectors for the wind in Figure 3.1. As is clear from this figure,
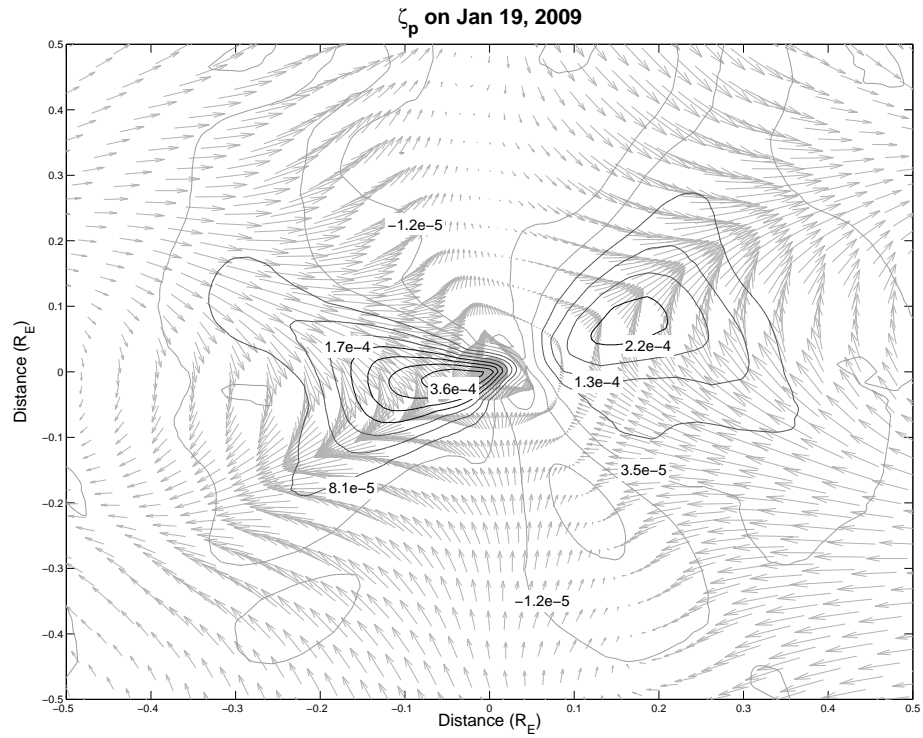
Figure 3.1: Shows contours of the ζ_p field plotted over wind velocity vectors for January 2, 2009 to confirm the accuracy of vorticity calculations. Labels for contour values are given in units of s^{-1}.

the peaks in the vorticity coincide with the area with the strongest curvature in the wind which is as expected.

Since the data is over the pole, and only the general form of the vortex is being described, ζ_p is computed in cylindrical coordinates. The vertical component of the curl of the wind in cylindrical coordinates is defined as

$$(\nabla \times \vec{V}) \cdot \hat{e}_z = \frac{1}{r} \left(\frac{\partial(rV_\theta)}{\partial r} - \frac{\partial V_r}{\partial \theta} \right) \tag{3.1}$$

The analysis of the vortex will be done using the zonal wind (u) and the meridional wind (v) on a 10 hPa pressure surface, again from the NCEP/NCAR Reanalysis dataset. Substituting these variables into Equation 3.1 gives the definition of vorticity used in this analysis.

$$\zeta_p = \frac{1}{r} \left(\frac{\partial(ru)}{\partial r} - \frac{\partial v}{\partial \theta} \right) + f \tag{3.2}$$

The f in this equation is the Coriolis Parameter shown in Equation 1.9. The differential angle $(\partial\theta)$ used in this is taken from the data-set as $2.5°$ latitude, or 0.0436 radians. The differential distance (∂r) is the arc length of $2.5°$ longitude at 10 hPa, approximated to be 278.70 km. All distances and wind velocities are scaled by the radius of the Earth, which is assumed to be 6356.75 km, so the numerical differentiation converges. This makes the new value of $\partial r = 0.0438$. Due to the $\frac{1}{r}$ dependence in Equation 3.2, the vorticity can not be numerically approximated for the point where $r = 0$. Therefore, the point at the pole is originally disregarded in

the vorticity computations, as shown in Figure 3.2. The numerical differentiation for vorticity are done primarily using the center difference method shown in Equation 3.3. However, differentiation with respect to r around the data hole and at the outer edge is done with forward (Equation 3.4) and backward (Equation 3.5) differentiation, respectively.

$$f'_j = \frac{f_{j+1} - f_{j-1}}{2h} + \mathcal{O}(h^2) \tag{3.3}$$

$$f'_j = \frac{-f_{j+2} + 4f_{j+1} - 3f_j}{2h} + \mathcal{O}(h^2) \tag{3.4}$$

$$f'_j = \frac{3f_j - 4f_{j-1} + f_{j-2}}{2h} + \mathcal{O}(h^2) \tag{3.5}$$

In order to fill the hole at $r = 0$ in the ζ_p field, the relationship between circulation and vorticity (described in Section 1.2.2) is applied. This means an approximation for vorticity at the pole can be found by summing the u wind values at $87.5\,°N$ (the last value before the pole) for every longitude, mulitplying by the circumferance of the circle made at that latitude, then dividing by the area of that same circle. The addition of this point at the pole is shown in Figure 3.3. This still causes some error at the pole because it has an extremely low resolution compared to the surrounding points, and a less acculate approximation method.
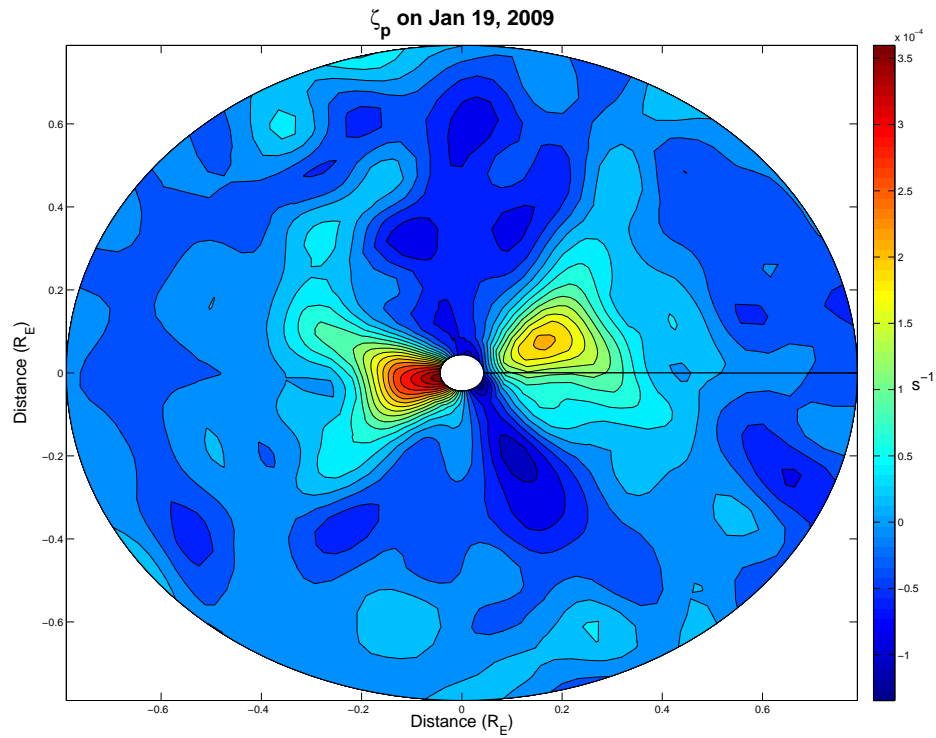
Figure 3.2: Graph of vorticity over the pole in cylindrical coordinates on January 19, 2009 showing two peaks, which represents a split vortex. Point at pole is omitted for intial calculation.

The error around the pole can have the effect of cutting out the center of a strong vortex making any secondary vortices seem much more relatively significant. This is why 4x-daily data is used, so anomalies created by the error can be ignored using flags in the code. There are two flags in the code to check for error, one checking if the circulation value for the main vortex is too low, and another checking if the ratio of two vortexes is too high. If either of these flags are triggered the ζ_p is disregarded. Using the 4x-daily data, it is still a safe assumption that at least two ζ_p fields for any split event will meet the qualification outlined earlier in this chapter without triggering a flag. However, it is not uncommon for events to initially be wrongly classified. This is why the classification must either be confirmed or corrected through observation of the event epoch.

The general form of the vortex can be observed using just the ζ_p field, as is demonstrated in Figures 3.2 and 3.3 which shows a split vortex. However, it is necessary to define the edge of a vortex in the this field for computing the number or vortexes and their strengths. In order to achieve this $\nabla^2 \zeta_p$ is computed.

Originally, $\nabla^2 \zeta_p$ was also computed in cylindrical coordinates, but due to the $\frac{1}{r^2}$ factor there was a large amount of error around the pole making the data useless. To avoid this problem ζ_p is interpolated from cylindrical coordinates into Cartesian coordinates, including the point at the pole. The differential distance used in the new coordinate system is $dx = dy = \frac{dr}{4}$, and the new ζ_p field is shown in Figure 3.3.

Finally, $\nabla^2 \zeta_p$ is computed in Cartesian coordinates based on the definition

$$\nabla^2 \zeta_p = \frac{\partial^2 \zeta_p}{\partial x^2} + \frac{\partial^2 \zeta_p}{\partial y^2} \tag{3.6}$$

29
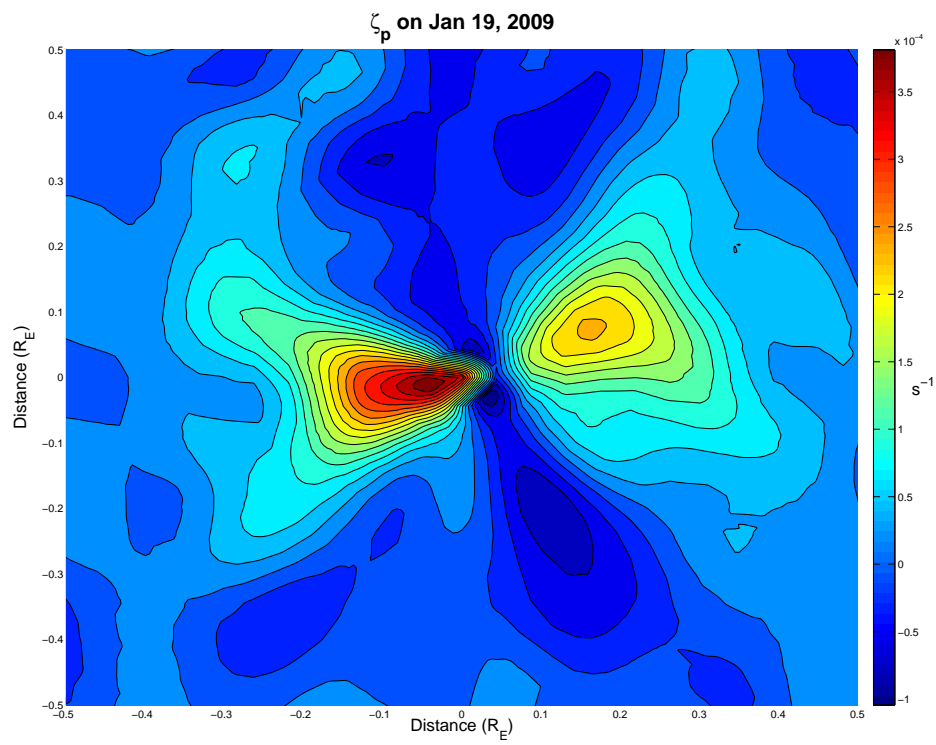
Figure 3.3: Same data as shown in Figure 3.2 only interpolated into Cartesian coor-
dinates, and with the point at the pole added.

The vertical derivative is disregarded since the data all exists on a pressure surface which is approximated to be all at the same altitude. The differentiation is approximated at every point using the second order center difference method.

$$f_j'' = \frac{f_{j+1} - 2f_j + f_{j-1}}{h^2} + \mathcal{O}(h^2) \tag{3.7}$$
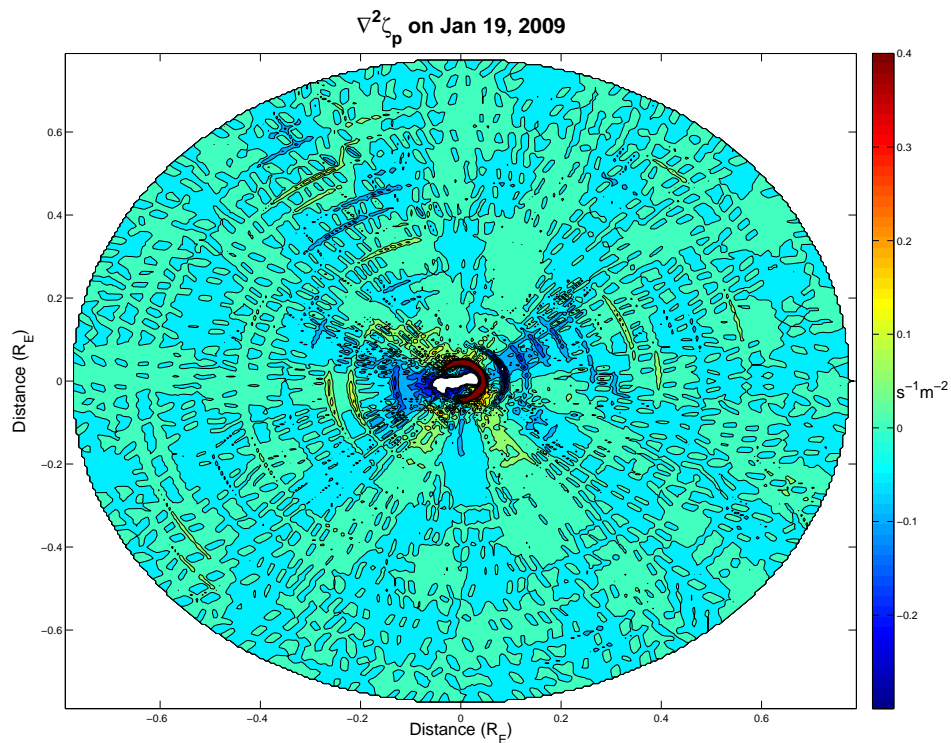
Figure 3.4: Graph of Laplacian of vorticity over the pole on January 19, 2009

Theoretically, the edge of a vortex would be defined as the contour where $\nabla^2 \zeta_p = 0$; unfortunately, this data is far too noisy for that method as seen in Figure 3.4. Instead,

the more rigorous method described earlier in this chapter will be used.

After the ζ_p field is calculated, the point where ζ_p reaches its maximum value is recorded as Z_{max}. The point is considered the center of the main vortex, and any viable vortex edge must enclose this point. Next, the ζ_p field is contoured into n_c evenly spaced contours, for this project $n_c = 20$. These contours are recorded, and the mean of the absolute value of $\nabla^2 \zeta_p$ is calculated along the path of each contour. The contour with the lowest mean absolute value of $\nabla^2 \zeta_p$ that includes Z_{max} is considered the edge of the main vortex, and the value of this contour is denoted as Z_e. Any closed contour made at Z_e is considered to be the edge of a vortex. If Z_e is defined at too low a ζ_p value then it could identify errors toward the edge of the field as part of a vortex. To avoid this, Z_e must be greater than a noise floor, which is set at $7 \times 10^{-5} s^{-1}$. If Z_e is originally below the noise floor, the value is dismissed and the next most appropriate value is picked.

After an appropriate value for Z_e is established it is time to determine the classification. The classification algorithm defaultly considers events displacements, and the classification is changed to a split if multiple vortices are identified. The ζ_p field is contoured again, this time only at Z_e, and the number of closed contours are counted. If there is only one contour the event is considered a displacement, and the classification is done. However, if there are multiple contours, as in Figures 3.5 and 3.6, then the relative strength of each vortex is compared to determine if the SSW is a split event. Circulation is used as a measure for the strength of each vortex, and as explained in Section 1.2.2 Stokes' theorem relates circulation to vorticity. This means the strength of each vortex is approximated simply by summing all the ζ_p contained in each contour. If the ratio of the strength of the two strongest vortices ≥ 0.5 on more
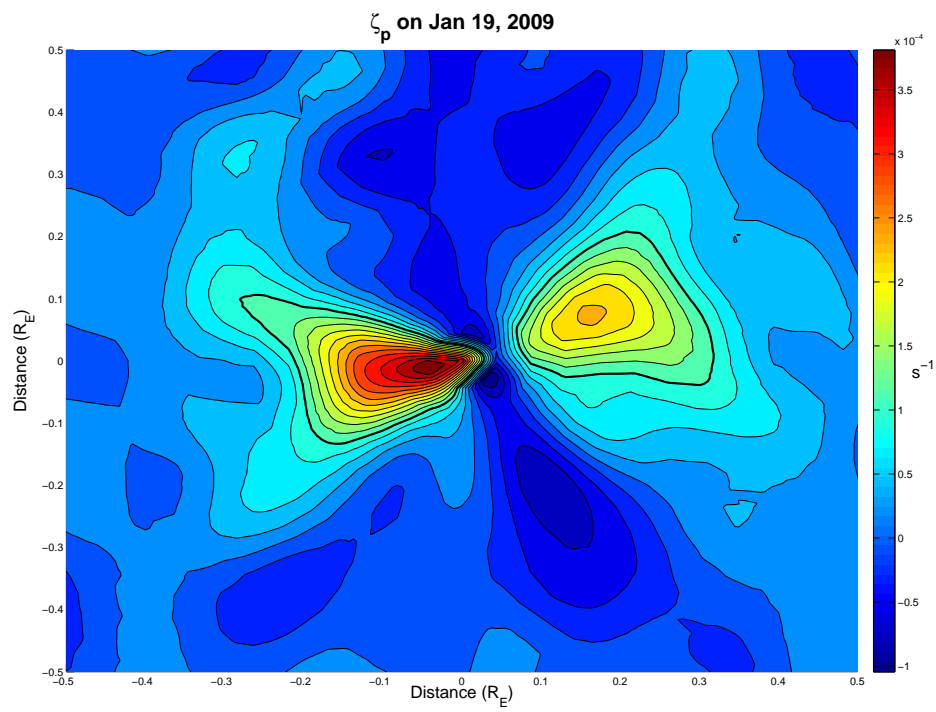
Figure 3.5: Same data as shown in Figure 3.3 with the vortex edge (Z_e) identified.
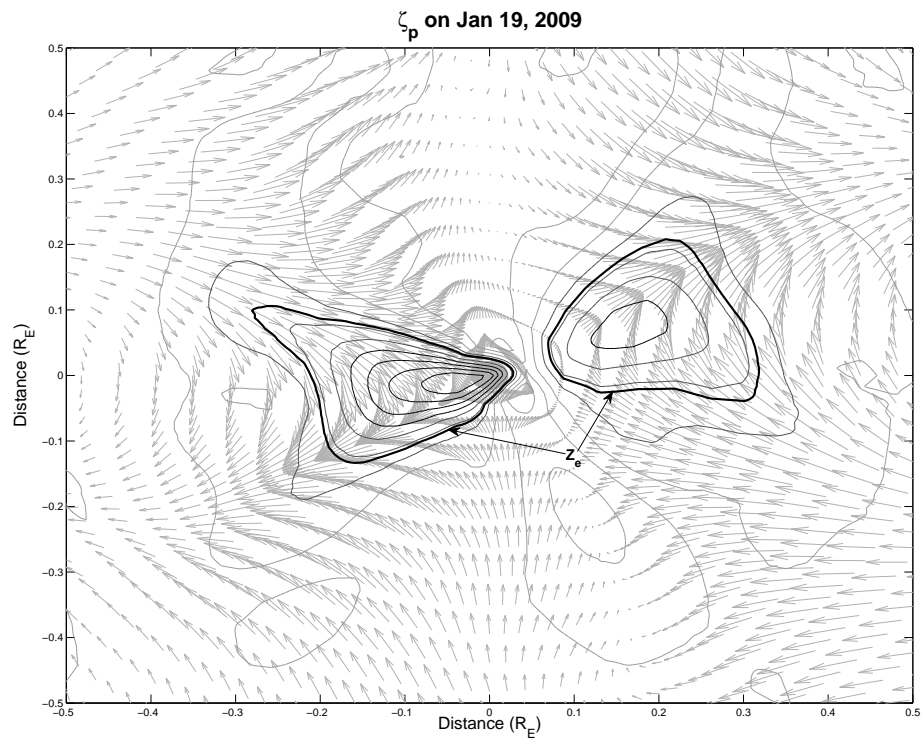
Figure 3.6: Same data as shown in Figure 3.1 with the vortex edge (Z_e) identified. The value of Z_e is approximately $1.14 \times 10^{-4} s^{-1}$ for the data shown.

than one field analyzed then the SSW is classified as a split event. A vortex ratio of 0.78 is found for ζ_p field displayed in Figures 3.5 and 3.6. Finally, as explained above, to confirm the classification of each SSW event the ζ_p field is manually inspected, and the day that the field best demonstrates the appropriate classification is recorded as the event epoch.

Chapter 4

Results: SSW events between

1978-2010

NCEP/NCAR Reanalysis data for the 33 winter seasons spanning November 1, 1978 to March 15, 2011 were analyzed as described in Chapter 2 and Chapter 3. The results are presented in Table 4.1 with previously unreported events in bold. During the period analyzed 41 SSWs were identified, which gives an average rate of 1.24 events/year. From the identified events, 19 were classified as displacements while 22 were classified as splits, giving a displacement/split ratio of 0.86. To demonstrate the similarity between the new and the previously identified events, Figure 4.1 shows five previously known events and Figure 4.2 shows five new events.

The averages of the duration and temperature parameters are presented in Table 4.2. The average ΔT over the 41 events reported here is 12 K with an standard deviation of nearly 5 K. That is, the average 10 hPa-level temperature during an SSW event is 12 K above the average temperature during the two weeks preceding

Table 4.1: Classified SSW events spanning 1978-2010 with previously unreported events in bold. Classifications of "D" and "S" denote displacement and split events, respectively. Dates are given in day of year (DOY).

Year	Central Date (DOY)	Event Duration (Days)	T_{ave} (K)	T_{max} (K)	ΔT (K)	$ZMZW_{max}$ (m/s)	Class	Event Epoch (DOY)
1978	**340**	**14.00**	**219**	**225**	**13**	**4.5**	**S**	**343.00**
1979	51	50.50	227	235	15	13.6	S	50.50
1979	**329**	**29.50**	**209**	**216**	**-1**	**0.3**	**D**	**327.25**
1980	58	34.00	233	246	17	9.9	D	63.00
1981	36	28.25	230	246	12	1.3	D	38.00
1981	336	4.25	213	214	5	11.0	D	337.00
1982	**26**	**6.50**	**236**	**240**	**16**	**-5.4**	**S**	**22.50**
1983	**82**	**54.50**	**231**	**241**	**14**	**0.2**	**D**	**74.00**
1984	54	40.00	231	242	11	11.7	D	59.50
1984	363	14.50	230	239	13	17.5	S	365.00
1986	**77**	**42.75**	**230**	**245**	**12**	**14.4**	**S**	**77.00**
1987	22	58.00	224	235	8	22.5	D	19.50
1987	340	11.00	230	235	13	30.5	S/**D**	342.00
1988	73	31.75	233	241	15	3.9	S	72.00
1989	52	42.25	230	242	15	13.5	S	49.00
1990	**43**	**54.75**	**226**	**241**	**9**	**-4.6**	**D**	**49.25**
1991	**35**	**27.50**	**226**	**239**	**8**	**-0.6**	**S**	**36.75**
1992	**13**	**44.50**	**228**	**241**	**11**	**-2.3**	**D**	**9.00**
1993	**66**	**47.75**	**229**	**235**	**6**	**0.4**	**S**	**74.00**
1994	**3**	**5.25**	**227**	**229**	**13**	**-2.4**	**D**	**3.00**
1994	**88**	**12.75**	**225**	**228**	**6**	**-5.4**	**S**	**83.25**
1995	**34**	**21.25**	**233**	**241**	**14**	**1.1**	**D**	**36.00**
1995	**81**	**5.25**	**215**	**217**	**0**	**1.0**	**D**	**85.50**
1996	**89**	**61.50**	**227**	**236**	**8**	**-3.4**	**D**	**53.75**
1997	**358**	**33.75**	**222**	**231**	**10**	**5.2**	**S**	**362.50**
1998	**87**	**47.50**	**225**	**232**	**12**	**4.4**	**S**	**39.00**
1998	348	9.25	229	235	17	22.8	D	345.00
1999	55	9.75	237	241	21	18.3	S	56.50
2000	79	64.75	224	235	10	4.2	D	77.00
2000	**355**	**13.00**	**223**	**227**	**8**	**-5.7**	**S**	**358.00**
2001	41	23.50	228	232	18	14.3	S	38.00
2001	361	35.75	224	237	14	7.7	D	357.75
2002	47	20.50	229	234	13	-0.1	D/**S**	49.50
2003	17	77.25	223	232	10	12.9	S	66.50
2004	3	25.75	227	232	18	11.8	S	4.00
2005	70	29.25	229	233	11	12.9	S	66.50
2006	20	34.50	227	236	14	24.1	S	18.50
2007	53	55.50	223	231	8	9.7	D	57.00
2008	52	54.00	225	238	14	13.9	D	57.00
2009	23	23.75	231	251	23	30.2	S	19.50
2010	26	17.25	228	235	21	7.1	S	28.00

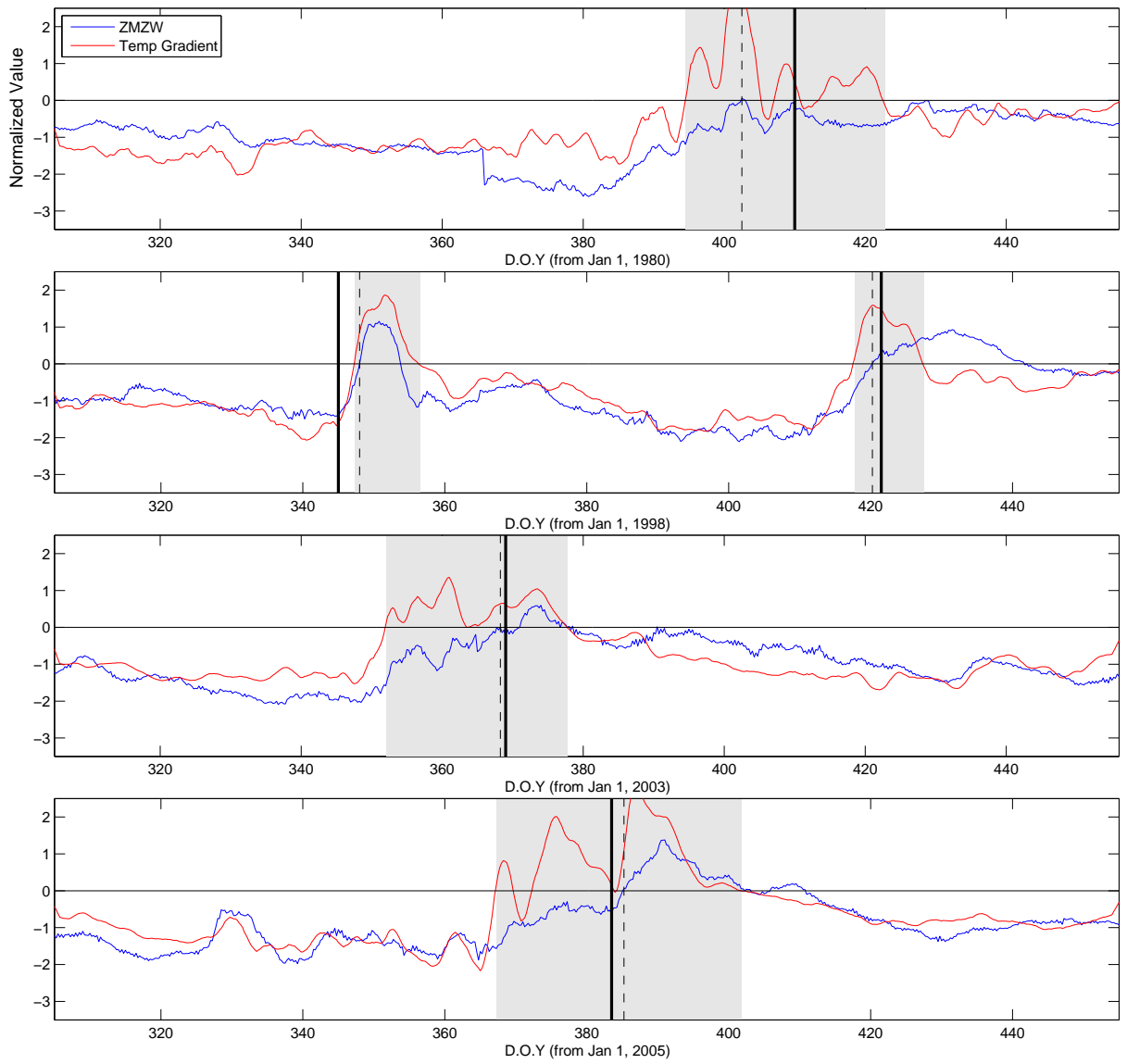Figure 4.1: Identification parameters for 4 winter seasons with previously recorded events. The duration of each event is shaded in grey, central dates are marked by a dashed vertical line, and event epochs are marked by a solid vertical line. All values are normalized by average absolute value.
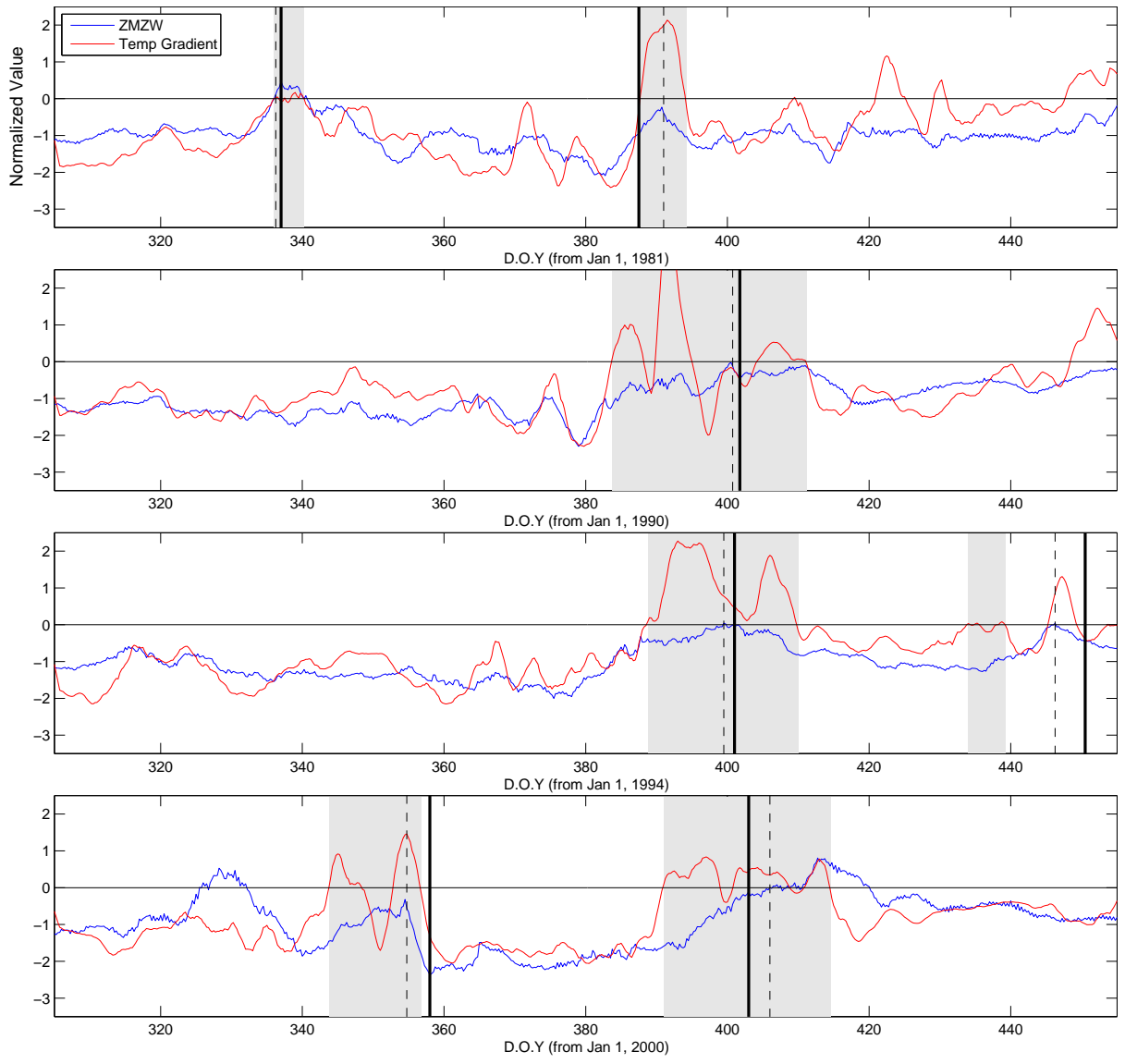
Figure 4.2: Similar to Figure 4.1 only displaying 4 winter seasons each with at least one previously unidentified events

Table 4.2: Duration, temperature, and wind parameters are averaged together for SSW events with similar classifications.

	All SSWs	Dev	Split	Displaced
Duration (Days)	32	18.7	29	35
T_{ave} (K)	227	5.4	228	225
T_{max} (K)	235	7.6	236	235
ΔT (K)	12	4.5	13	11
$ZMZW_{max}$ (m/s)	11.2	8.4	12.4	9.9

the event. The average maximum temperature at 10 hPa during an SSW event is 235 K with a standard deviation of 8 K. The average event duration is 32 days, but this value is highly variable with a standard deviation of 19 days. The maximum ZMZW during each event is also averaged together and found to be 11 m/s in the easterly direction with a standard deviation of 8 m/s. When compared to the corresponding values observed for displacement events, split events have a ΔT almost 2 degrees higher, a T_{ave} 3 degrees higher, a T_{max} one degree higher, a maximum ZMZW 3.5 m/s greater easterly, and 6-day shorter duration. This means that split events general cause a slightly greater atmospheric disturbance then displacement events despite being shorter.

There are two events that are confirmed by Charlton and Polvani (2007), but are given different classifications when the method described in Chapter 3 is used. The first of these is the December 1987 event which was originally classified on as a split, but is classified as a displacement. Second, the February 2002 was classified as a displacement previously, and is classified as a split here. For both of these events, along with every event, the classification is confirmed by observation of the ζ_p field on the event epoch. Also, both classifications are listed for these events with the new

classification in bold, and when events are grouped by class the new classification is used.

SSW events were also identified using the definition of minor warmings and major warmings. All major warming events between November 1, 1978 and March 15, 2011 are presented in Table 4.3. The central date for these events is the first time the ZMZW at $70 - 80\,^\circ$N becomes easterly. For the 33 winter seasons there were 28 major warming events identified giving a rate of 0.85 events/year. There are six major warming events identified here that are not previously reported, and those events are listed in bold. Minor warming events for the same period are identified based solely on the reversal of the temperature gradient with no duration requirements, and they are presented in Table 4.4. The central date here is the time when the meridianol temperature gradient reaches its maximum value, and the duration and maximum ZMZW values are also recorded for each event. Minor warmings listed in bold are not included in Table 4.1. There are 49 minor warming events identified which gives a rate of 1.48 events/year over the period analyzed.

Table 4.3: All major warming events from 1978-2010 using ZMZW at $70 - 80\,^\circ$ N. Central Dates are given in DOY, and previously unreported events are listed in bold.

Year	Central Date
1978	**340**
1979	51
1979	**329**
1980	58
1981	36
1981	336
1984	54
1984	363
1987	22
1987	340
1988	73
1989	52
1995	**34**
1996	**323**
1997	**358**
1998	348
1999	55
2000	**325**
2001	41
2001	361
2003	17
2004	3
2005	70
2006	20
2007	53
2008	52
2009	23
2010	26

Table 4.4: All minor warming events from 1978-2010 are listed along with their duration and the maximum ZMZW around the duration. Events that are not included in Table 4.1 are listed in bold.

Year	Central Date (DOY)	Duration (Days)	$ZMZW_{max}$ (m/s)
1978	354	14.00	4.5
1979	57	50.50	13.6
1979	330	29.50	0.3
1980	60	34.00	9.9
1981	35	28.25	1.3
1981	339	4.25	11.0
1982	26	6.50	-5.4
1982	**57**	**21.50**	**-15.1**
1982	**364**	**1.25**	**-30.0**
1983	56	54.50	0.2
1984	62	40.00	11.7
1984	**344**	**1.25**	**-27.6**
1984	364	14.50	17.5
1986	**20**	**3.25**	**-27.4**
1986	79	42.75	14.4
1987	34	58.25	22.5
1987	343	11.00	30.5
1988	88	31.75	3.9
1989	43	42.25	13.5
1990	40	54.75	-4.7
1991	26	27.50	-0.6
1992	11	44.50	-2.3
1993	62	47.75	-0.4
1994	2	5.25	-2.4
1994	70	12.75	-5.4
1995	28	21.25	1.1
1995	74	5.25	1.0
1996	68	61.50	-3.4
1997	359	33.75	5.2
1998	51	47.50	4.4
1998	351	9.25	22.8
1999	55	9.75	18.3
2000	83	64.75	4.2
2000	355	13.00	-5.7
2001	32	23.50	14.3
2001	358	35.75	7.7
2002	47	20.50	-0.1
2003	16	77.25	2.8
2004	361	25.75	11.7
2005	**32**	**0.75**	**-32.9**
2005	54	29.25	12.9
2006	22	34.50	24.1
2007	**2**	**5.75**	**-28.4**
2007	62	55.50	9.7
2008	24	54.00	13.9
2009	22	23.75	30.3
2010	26	17.25	7.1
2011	**32**	**3.25**	**-20.1**
2011	**84**	**17.25**	**-11.9**

43

Chapter 5

Discussion

The results presented in Chapter 4 show that SSWs were identified at a rate of 1.24 events/year, or about 12 events every decade with the new identification method. This is nearly double the rate of 0.62 events/year as reported by Charlton and Polvani (2007). The reason for the disparity between these two rates is their report does not include the smaller magnitude events during the period from 1990-1997 along with several in the 1980's. These new events were identified because the threshold for ZMZW was changed, or because the ZMZW from $70 - 80\,^{\circ}$N is more correlated to disturbances. The displacement/split ratio of 0.86 reported here is similar to the value of 1.18 reported by Charlton and Polvani (2007); however, this new ratio indicates a higher probability of split events. Split type events also seem to be occurring with increasing frequency with 8 of the 12 events occuring in the 2000's classified as splits.

There are also some noteable points to make about the list of minor warmings and major warmings listed in Chapter 4. First with the major warmings, presented in Table 4.3, there is one event during December 1996 that does not have any distur-

bance in the meridional temperature gradient associated with it, and is therefore not included in the general list of SSWs in Table 4.1. With regard to the minor warming events, presented in Table 4.4, it is important to note the differences of the events in bold which are not included in the general list of events. The reason these events are not included in the final list is because there are no disturbances in the ZMZW associated with them. This is demonstrated by the fact that the maximum ZMZW associated with these events is never below 12 m/s, and usually around 20 m/s in the westerly direction, significantly higher then the threshold used here for identifying events. Also, every minor warming event with a duration shorter then four days was eliminated because of the lack of ZMZW disturbance. This implies that a warming event must be at least four days long to be associated with a significant dynamic disturbance.

Significant variability in the occurrence rate of SSW events has been reported and investigated in several recent papers (Lu et al., 2008; Schimanke et al., 2011). There have also been variation on this with several papers reporting a recent increase in the occurrence rate (Charlton-Perez et al., 2008; McLandress and Shepherd, 2009). However, if the events shown in Table 4.1 are seasonally-binned to the first year of the season then grouped by decade for the 1980's, 1990's, and 2000's, there are 12, 13, and 12 events respectively. This shows a long term consistency in the rate throughout the three decades analyzed. Perhaps more interesting is that linear regression analysis of all the seasonally-binned events, as seen in Figure 5.1, actually shows the rate of events per year decreasing by about 2 less events per century. Using a goodness of fit test on this linear regression, the upper bound of the rate is nearly zero, and only slightly positive. Thus there is no significant evidence of a recent increase in the rate.
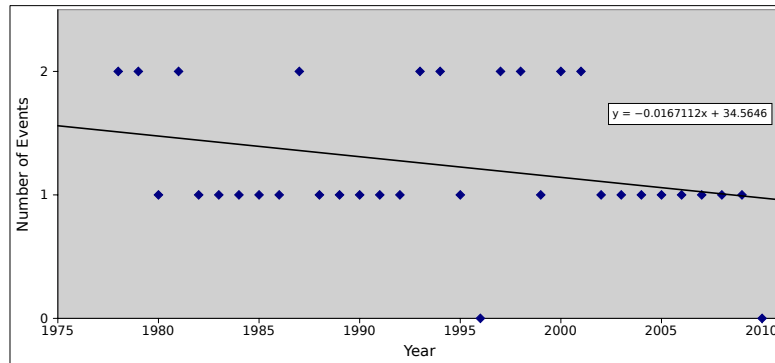
45

Figure 5.1: Number of SSW events graphed versus their seasonally-binned year along with a best-fit line showing a decrease in the occurence rate of -0.017 events/year. The lower and upper bounds of this slope with 95% confidence are -0.0371 and 0.0036, respectively.

As a check for consistency and to gain further insight, the identification schemes for major and minor warming are adjusted, and events are identified based on these variations. First, minor warmings are identified with the more traditional requirement that the meridional temperature gradient must remain continuously reversed for a period of at least 5 days. Using this method there are 12 events that are not identified that were included in Table 4.4. This changes the rate for minor warming events to 1.12 events/year. Next, the major warmings are identified by the reversal of the ZMZW at 60 °N, as is traditionally used. With this method there are five events listed in Table 4.3 that are no longer included, all of the bold events from the table with the exception of the Febraury 1995 event. This brings the rate of major warmings down to 0.70 events/year which is similar to the rate found by Charlton and Polvani (2007) because this is the same method used in their work.

Chapter 6

Future Work and Present Conclusions

The effects of SSW events on troposheric and stratospheric wind patterns has been well documented. However, the effects of these events on upper regions of the atmosphere are not yet well understood. In recent years there have been several papers reporting an unusual occurrences in the upper atmosphere that coincided with SSW events. These often focus on the events in January of 2008 and 2009, when a global effort was made to attempt to record data during the likely time of an event. Using the more complete list of events in Chapter 4, it is possible to find available data that coincides with more distant SSWs, and to better characterize what is associated with an SSW and what was due to other sources of dynamic variability.

6.1   Vertical Drift

One example of anomalous data in the upper atmosphere coinciding with an SSW was reported by Chau et al. (2009). They reported an unusual increase in the daytime vertical drift in the F-region of the ionosphere at the Jicamarca Radio Observatory (JRO) ($12\,^{\circ}$ S, $77\,^{\circ}$ W) during the end of January 2008, suggesting a possible correlation between the increased vertical drift and the SSW that occurred at the same time, possibly due to a change in the Earth's electric field. This is intriguing and counterintuitive, because one would not necessarily expect to an event occurring over the pole to have a pronounced affect at low latitudes.

The data used in this section all comes from the Madrigal website, filtered specifically for only the relevant data. The method used in this analysis involved averaging all vertical drift values from 200-400 km to achieve an average for the entire F-region. The ion drift is used since that is considered to be closely related to the neutral drift, and only the daytime (0630-1830) is used because that is the less naturally variable then other times. The KP and F10.7 are also recorded with the JRO data, they represent the fluctuation in Earth's magnetic field and the solar intensity respectively, and can have a strong impact on vertical drift.

In Figures 6.1 and 6.2 the results of Chau et al. (2009) are recreated to confirm that a self written Matlab code can indicate any anomalies in vertical drift. As is clear from both of these figures, there appears to be a dramatic increase in the early morning vertical drift, especially around January 23. This is basically the same time that warming in the high latitude stratosphere is most intense, so the theory is that this increase in drift is related to the SSW. There were four other occasions in which
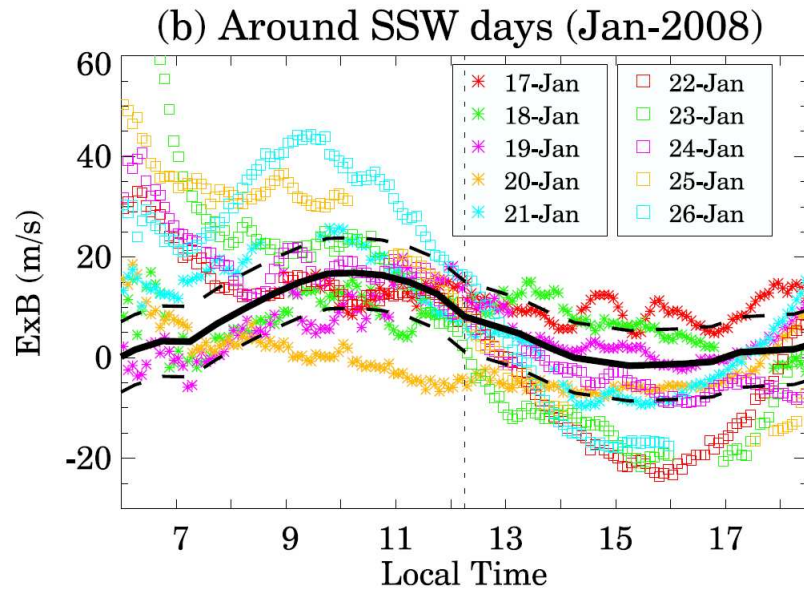
Figure 6.1: Graph of vertical drift versus local time on days surrounding the January 2008 SSW event from Chau et al. (2009)
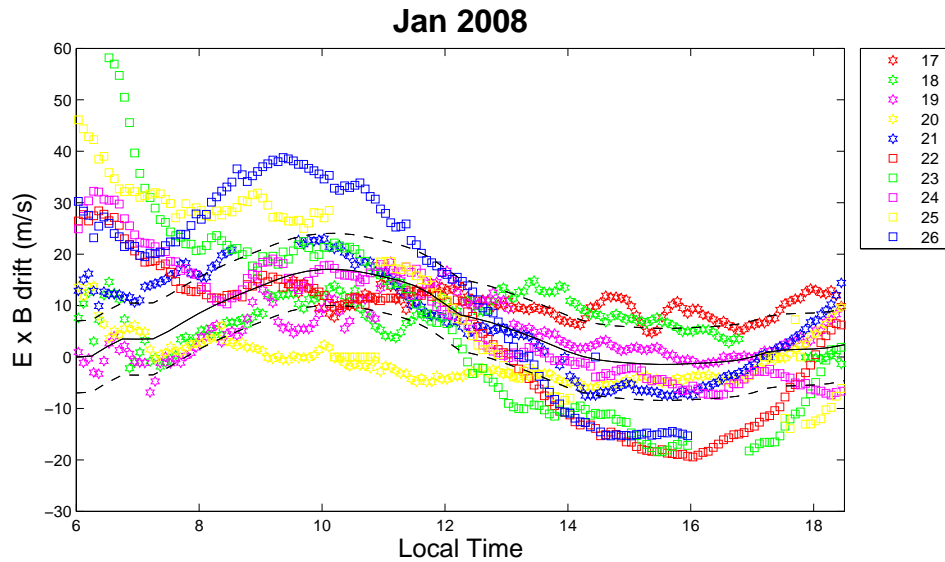

Figure 6.2: A recreation of the results displayed in Figure 6.1

some JRO data was available around the time of an SSW event: December 2000, December 2003, January 2009, and January 2010.
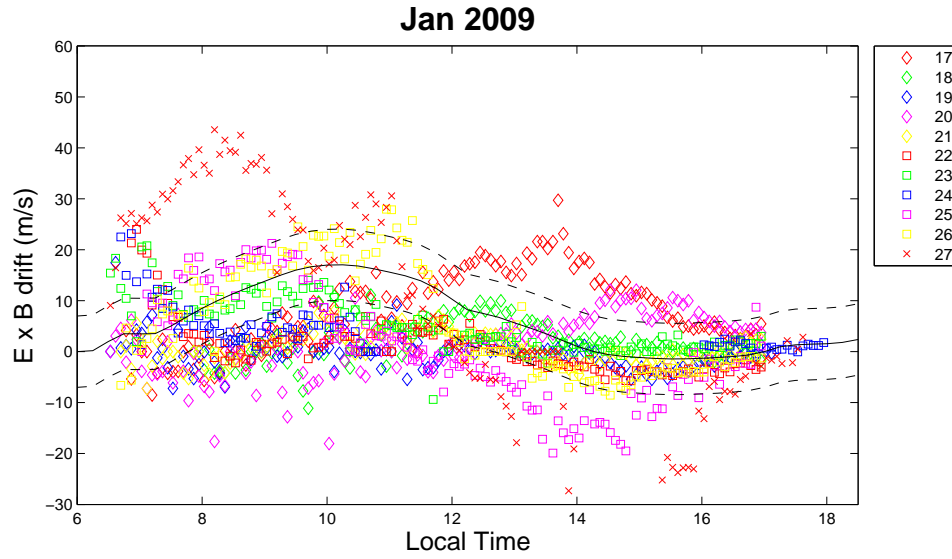

Figure 6.3: A graph of vertical drift versus local time spanning January 17 - 27, 2009
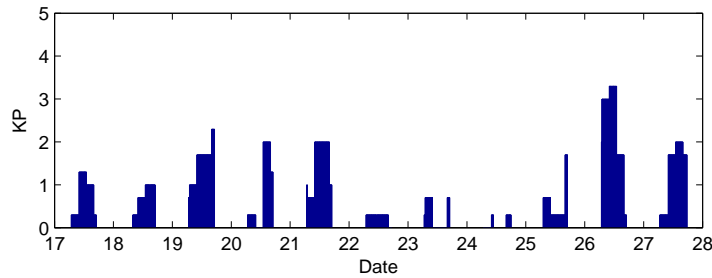

Figure 6.4: KP index for the time period shown in Figure 6.3

The JRO data for December 2000 and December 2003 are not very useful for these purposes because these dates are closer to a solar maximum, corresponding to high values on the F10.7 index. However, the January 2009 and January 2010 events

50

are closer to a solar minimun and have F10.7 values approximately the same as the event on January 2008. The data from January 2009, displayed in Figure 6.3, shows vertical drift for for the date surround an SSW event of that same season. There does appear to be a slight increase in the early morning vertical drift on the 27th; although, Figure 6.4 shows an increase in the Earth's magnetic field at this time. This combined with the fact that the warming in the stratosphere was most dramatic around the 22nd implies that the warming had little effect on the vertical drift. This conclusion is demonstrated again during the January 2010 SSW (Figure 6.5) where there is very little variability from the expected drift patterns.
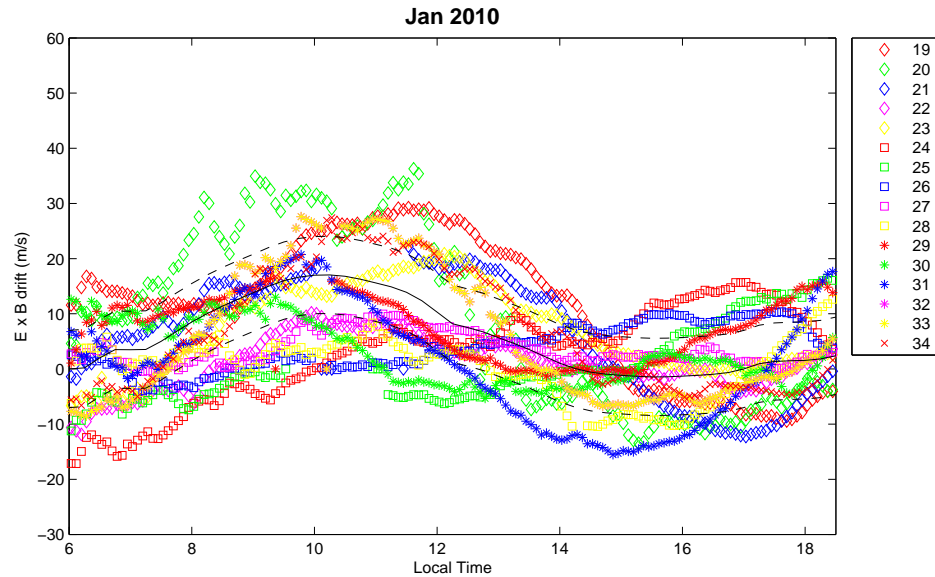

Figure 6.5: A graph of vertical drift versus local time spanning January 19 - Febraury 3, 2010. (Days counted from January 1)

6.2 Mesospheric Signals

The most often studied, and best understood effect of SSW events on the upper atmosphere is a cooling of temperature in the mesospheric and lower thermospheric region (MLT). This cooling was originally thought to be directly correlated to the warming in the stratosphere; however, it was shown by Azeem et al. (2005) that this cooling in the mesosphere can actually precede the warming by several days. To demonstrate this, mesospheric temperature data is used from Embry-Riddle's Space Physics Research Lab (SPRL). Data for temperature can be measured very accurately for a specific region in the mesophere using the OH(3,1) airglow data (Sivjee and Hamwey, 1987). Airglow data is available for three sites in SPRL: Longyearbyen (78° N, 15° E), Resolute Bay (74° N, 295°55$'$ W), and Sondrestrom (67° N, 15°33$'$ E). There are very few SSW events that occur during a time data from all three sites is available; one of these events is during December 1998 and is presented in Figure 6.6. The average for the mesospheric temperature (green line) at these three sites is acheived through a combination of averaging together local points, and splining over holes in the data.

This temperature data can be compared to NCEP/NCAR Reanalysis data in two separate ways. One way is to select temperature data points in the NCEP/NCAR Reanalysis data that correspond to the locations included in the SPRL data. This is done with the red lines in Figure 6.6. Another possibility is to average together the data from all three sites, and use it as a representation of the average mesospheric temperature over the northern polar region. This can be compared to the area-weighted temperature parameter described in Section 2.2. This is process demonstrated in
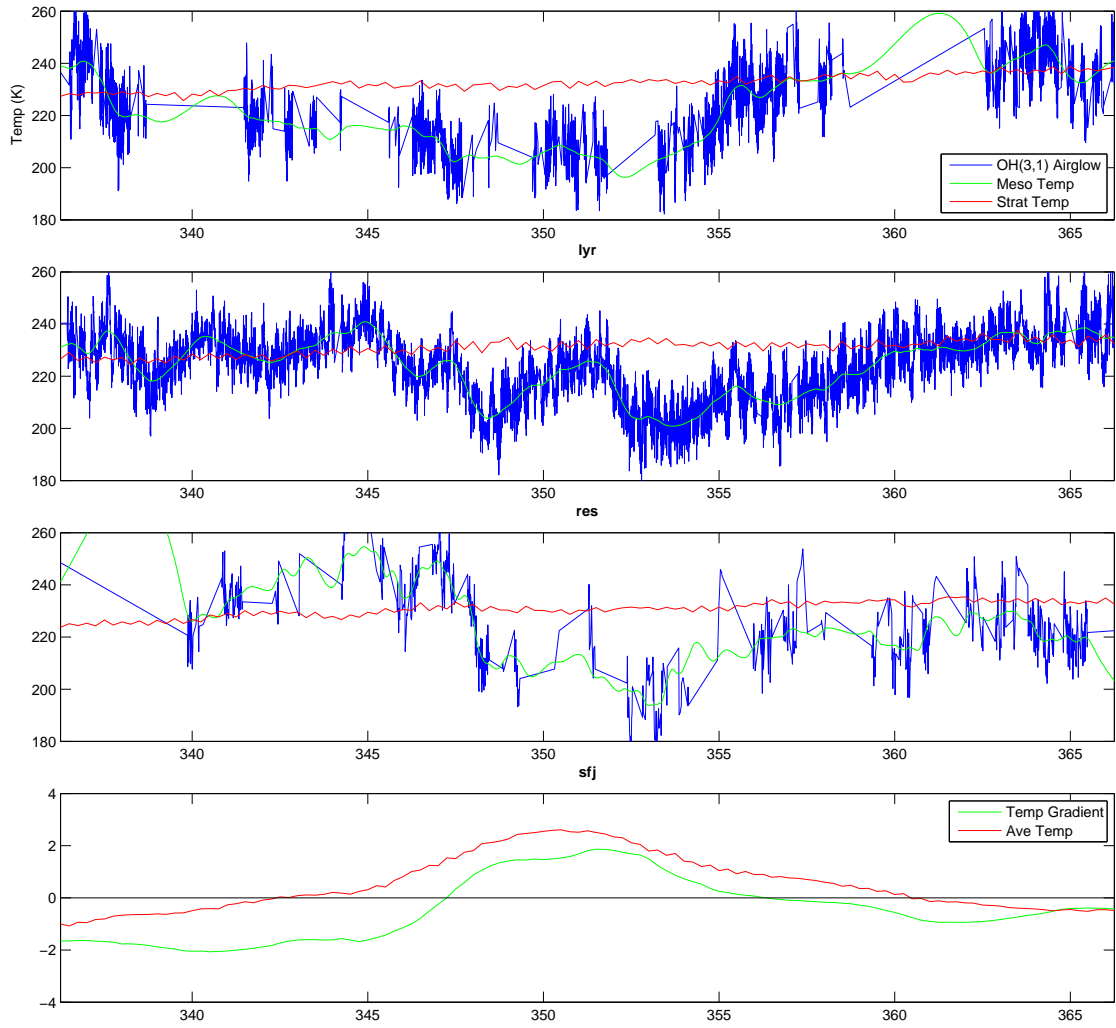
Figure 6.6: Temperature data for three different sites surround the December 1998 SSW event. Top three panel show Longyearbyen, Resolute Bay, and Sondrestrom respectively. The bottom panel shows the merdional temperature gradient and the area-weighted average temperature to demonstrate the SSW.

Figure 6.7, which shows cooling in the mesosphere coinciding with the stratospheric warming.
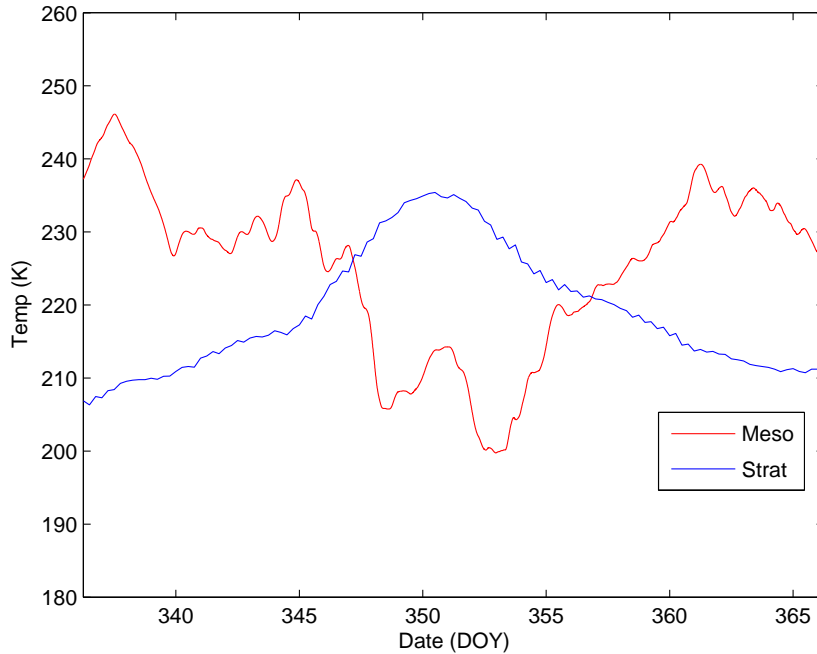

Figure 6.7: Mesospheric temperatures from all available sites are averaged together and compared to the area-weighted average temperature for the stratosphere around the SSW event of December 1998

As seen in Figure 6.8, the cooling in the mesosphere can begin and end at slightly different times based on location. Difference between temperature signals from different sites can be analyzed to determine if any phase delay exist between locations. This phase delay can be compared to the vortex morphology using the ζ_p field outlined in Chapter 3. This would hopefully reveal some relationship between the position of the vortex, and local temperature changes in the mesosphere. A quick MatLab analysis

of phase difference on the data presented in Figure 6.8 shows that Resolute Bay and Sondrestrom are approximately in phase, and both sites are about one day behind Longyearbyen.

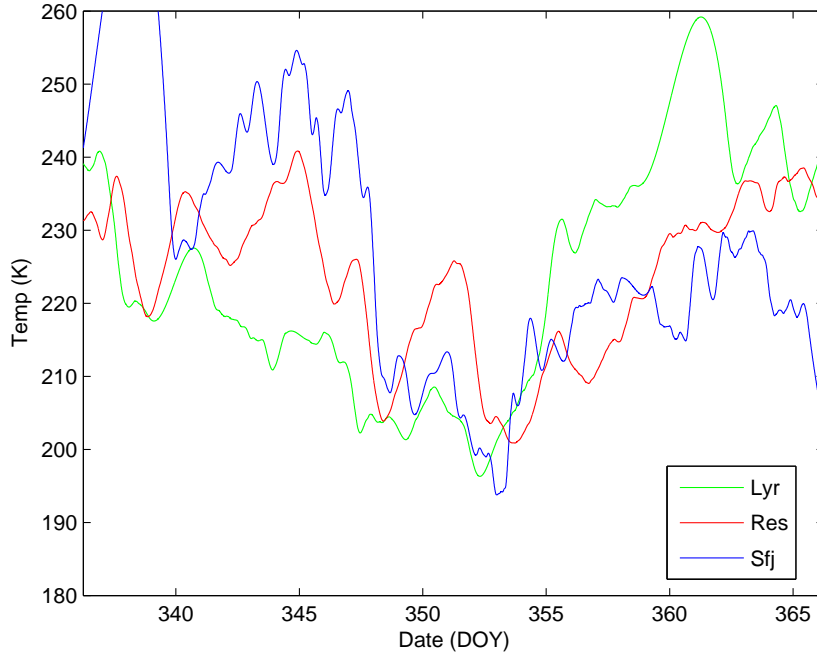Figure 6.8: Average mesospheric temperatures from three different locations are graphed together to demonstrate a slight phase difference between them

6.3   Conclusion

Sudden Stratospheric Warming events are one the most dramatic phenomenon to occur in the upper atmosphere, associated with temperature and wind anomalies that last several weeks and throughout multiple regions of the atmosphere. This

paper involved identifying SSWs through zonal wind and temperature data provided by the NCEP/NCAR reanalysis project. Events were identified by both the reversal of the meridional temperature gradient, and anomalies in the zonal mean zonal wind. Through this process there were 41 SSWs identified for 33 winter seasons analyzed, spanning from 1978-2011, giving an average rate of 1.24 events/year or approximately 12 events a decade. This value is a significant deviation from previous rates of SSWs produced, mostly due to a change in the magnitude of zonal wind anomaly necessary for a disturbance to qualify as an SSW. The most important quality about this new list of events is the consistency of the rate found. Each decade analyzed has approximately the same number of events, and a linear regression analysis of the number of events per year suggest that the rate of events may actually be decreasing slightly.

Each SSWs is also classified based on the evolution of the polar vortex throughout the event. Each event is either classified as a split or a displacement, based on whether the vortex divides as it is being deformed. The classification is done by analysis of the vorticity field on the days surrounding when the event was identified. Of the SSWs identified 19 were classified as displacements, and 22 were classified as splits. This gives a displacement/split ratio of 0.86, which is lower then previous ratio but still suggest close to a one-to-one ratio. There is, however, a recent increase in split events with the events in the last decade giving a 0.5 displacement/split ratio.

After an event is identified, additional analysis is done on the identification parameters. First, the duration of each event is recorded using the reversal of the temperature gradient. The average duration of an event is 32 days, but this value is highly variable with a standard deviation of almost 19 days. The average temperature throughout the duration of an event is also recorded (T_{ave}), as well as the maximum

temperature (T_{max}). This average temperature is then compared to the average temperature preceeding each event the the difference is recorded as ΔT. The average ΔT for all identified SSWs is 12 K, meaning an average SSW will cause polar temperatures to increase about 12 K above normal temperatures. Lastly, the maximum ZMZW value during an event is recorded. This is primarily to see if the magnitude of the ZMZW disturbance is great enough to be considered an SSW, and to compare these events to the traditional definition of a major warming event. These additional values are also compared for events of similar classification; when compared to displacements, it was found that split events have a shorter duration on average, but greater averaged values in every other parameter. This indicates that split events are generally associated with greater disturbances of stratospheric conditions.

Bibliography

S. M. I. Azeem, E. R. Talaat, G. G. Sivjee, H.-L. Liu, and R. G. Roble. Observational Study of the 4-Day Wave in the Mesosphere Preceding the Sudden Stratospheric Warming Events During 1995 and 2002. *Geophys. Res. Lett.*, 32:L15804, 2005. doi: 10.1029/2005GL023393.

M. P. Baldwin and T. J. Dunkerton. Propagation of the Arctic Oscillation from the stratosphere to the troposphere. *J. Geophys. Res.*, 104(D24):30937–30946, 1999. doi: 10.1029/1999JD900445.

M. P. Baldwin and J. R. Holton. Climatology of the stratospheric polar vortex and planetary wave breaking. *J. Atmos. Sci.*, 45:11231142, 1988. doi: 10.1175/1520-0469(1988)045.

A. J. Charlton and L. M. Polvani. A New Look at Stratospheric Sudden Warmings. Part I: Climatology and Modeling Benchmarks. *Journal of Climate*, 20:449–469, 2007.

A. J. Charlton-Perez, L. M. Polvani, J. Austin, and F. Li. The frequency and dynamics of stratospheric sudden warming. *J. Geophys. Res.*, 113:D16116, 2008. doi: 10.1029/2007JD009571.

J.L. Chau, B.G. Fejer, and L.P.Goncharenko. Quiet variability of equatorial e x b drifts during a sudden stratospheric warming event. *Geophys. Res. Lett.*, 36:L05101, 2009. doi: 10.1029/2008GL036785.

K. Coughlin and L. J. Gray. A Continuum of Sudden Stratospheric Warmings. *J. Atmos. Sci.*, 66:531–540, 2009. doi: 10.1175/2008JAS2792.1.

L. Goncharenko and S-R Zhang. Ionospheric signatures of sudden stratospheric warming: Ion temperature at middle latitude. *G. Res. Lett.*, 35(L21103), 2008. doi: 10.1029/2008GLL035684.

Mike Hickey. Ep 410 lecture notes, 2011.

John M. Hughes. Ep 410 lecture notes, 2008.

V. Limpasuvan, D. W. J. Thompson, and D. L. Hartmann. The life cycle of Northern Hemisphere stratospheric sudden warming. *J. Clim*, 17:2584–2596, 2004.

H. Lu, M. P. Baldwin, L. J. Gray, and M. J. Jarvis. Decadal-scale change in the effects of the QBO on the northern stratospheric polar vortex. *J. Geophys. Res.*, 113(D10114), 2008. doi: 10.1029/2007JD009647.

Mankin Mak. *Atmospheric Dynamics*. Cambridge University Press, New York, NY 10003, 2011.

O. Martius, L. M. Polvani, and H. C. Davies. Blocking precursors to stratospheric sudden warming events. *Geophys. Res. Lett.*, 36(L14806), 2009. doi: 10.1029/2009GL038776.

T. Matsuno. A dynamical model of the stratospheric sudden warming. *J. Atmos. Sci.*, 28:1479–1494, 1971.

R. M. McInturff. *Stratospheric warmings: Synoptic, dynamic and general-circulation aspects*. NASA Reference Publ. NASA-RP-1017, NASA, Natl. Meteorol. Cent., Washington, D. C., 1978.

C. McLandress and T. G. Shepherd. Impact of Climate Change on Stratospheric Sudden Warming as Simulated by the Canadian Middle Atmosphere Model. *Journal of Climate*, 22:5449–5463, 2009. doi: 10.1175/2009JCLI3069.1.

S. Schimanke, J. Korper, T. Spangehi, and U. Cubasch. Multi-decadal variability of sudden stratospheric warmings in an AOGCM. *Geophys. Res. Lett.*, 38(L01801), 2011. doi: 10.1029/2010GL045756.

G. G. Sivjee and R. M. Hamwey. Temperature and chemistry of the polar mesopause oh. *J. Geophys. Res.*, 92:4663–4672, 1987.

G. Sturaro. A closer look at the climatological discontinuities present in the NCEP/NCAR reanalysis temperature due to the introduction of satellite data. *Climate Dynamics*, 21:309–316, 2003. doi: 10.1007/s00382-003-0334-4.

M. Taguchi. Is there a statistical connection between stratospheric sudden warming and tropospheric blocking events? *J. Atmos. Sci.*, 65:1442–1454, 2008.

Y. Tomikawa. Persisitence of Easterly Wind during Major Stratospheric Sudden Warming. *Journal of Climate*, 23:5258–5267, 2010. doi: 10.1175/2010JCLI3507.1.

D. W. Waugh and L. M. Polvani. Stratospheric Polar Vortices. In L. M. Polvani, A. H. Sobel, and D. W. Waugh, editors, *The Stratosphere: Dynammics, Transport, and Chemistry, Geophysical Monograph 190*, pages 43–57. American Geophysical Union, Washington, DC, 2010.